

Cryogenic small-signal conversion with relaxation oscillations in Josephson junctions

Miha Furlan

Laboratory for Astrophysics, Paul Scherrer Institute, 5232 Villigen PSI, Switzerland

(Dated: December 2, 2024)

Broadband detection of small electronic signals from cryogenic devices, with the option of simple implementation for multiplexing, is often a highly desired, although non-trivial task. We investigate and demonstrate a small-signal analog-to-frequency conversion system based on relaxation oscillations in a single Josephson junction. Operation and stability conditions are derived, with special emphasis on noise analysis, showing the dominant noise sources to originate from fluctuation processes in the junction. At optimum conditions the circuit is found to deliver excellent noise performance over a broad dynamic range. Our simple models successfully apply within the regime of classical Josephson junction and circuit dynamics, which we confirm by experimental results. A discussion on possible applications includes a measurement of the response to a cryogenic radiation detector.

PACS numbers: 85.25.Oj, 85.25.Hv, 84.30.Qi, 74.40.+k

I. INTRODUCTION

Cryogenic devices are widely used in a broad range of applications like radiation detection, quantum cryptography, charge manipulation on the single-electron level, quantum Hall effect or in basic studies of mesoscopic transport. Measurement of the electronic properties of such devices usually requires sophisticated readout electronics. Detection schemes where the samples at cryogenic temperatures are remotely connected to room temperature electronics generally face the problem of reduced frequency bandwidth due to the impedance of long readout lines. In addition, the risk of noise pickup on the lines is intrinsically increased. Alternatively, signal readout relatively close to the sample can be accomplished with SQUID amplifiers, which perform very successfully in many cases but require a delicate setup (shielding) and are usually constrained to commercially available systems. Amplification or impedance transformation on-chip or very close to the sample is also possible with a HEMT, the dissipation of which may, however, quickly reach an unacceptable level.

In recent years it has been realized that probing the electronic transport in a cryogenic device with an RF signal^{1,2,3,4,5,6} may have considerable advantages compared to direct signal readout, mainly due to a substantial extension of the bandwidth. In those schemes the power of the reflected (or transmitted) RF signal from a properly tuned tank circuit is related to the electronic state of the device under test. The circuit needs to be carefully designed to minimize back-action on the cryogenic sample. Operation at microwave frequencies also naturally opens a potential way for frequency-domain multiplexing.^{7,8}

A promising new readout scheme, which we present in this paper, consists of an on-chip analog-to-frequency converter, delivering a frequency signal of large amplitude which is easily demodulated with standard room temperature (phase-locked loop) electronics. It has the advantages of both the direct signal readout close to the

sample and a large frequency bandwidth. Particularly, it is much easier to accurately analyze a frequency signal than to transmit a low-level analog signal through long readout lines and amplify it with room temperature equipment which typically shows inferior performance in terms of noise with increasing temperature. Our low-noise converter circuit is based on a hysteretic Josephson junction exhibiting relaxation oscillations. Related ideas using relaxation oscillations in Josephson junction were proposed for thermometry⁹ or direct radiation detection,¹⁰ both relying on the temperature dependence of quasiparticle population in the gap singularity peak of asymmetric junctions, and for the (double) relaxation oscillation SQUID,^{11,12,13} which is investigated and used as a magnetometer. In our case the circuit converts an analog current signal into a frequency with acceptable linearity over a broad operation bias and dynamic range.

In Sec. II we review the basic principle of a relaxation oscillation circuit and derive conditions for stable operation. Results from the model are illustrated with experimental data. A thorough noise analysis with implications for the circuit's readout resolution is given in Sec. III. An optimized low-noise configuration with numerical estimates is considered in Sec. IV, followed by a discussion on possible applications in Sec. V. As an example we demonstrate the readout of a cryogenic radiation detector. The paper concludes with Sec. VI.

II. PRINCIPLE OF OPERATION

We assume a Josephson device with normal resistance R_n , critical current I_c , junction capacitance C_j and superconducting energy gaps Δ_1, Δ_2 , where $0 < |\Delta_1 - \Delta_2| \ll \Delta_1 + \Delta_2 \doteq eV_g$. It shall be connected in series with an inductance L and both shunted with a resistor R_s , as shown schematically in Fig. 1. The circuit is eventually current biased by a large resistor $R_b \gg R_s$. A Josephson junction with a non-vanishing difference of the energy gaps shows a region of negative differential resis-

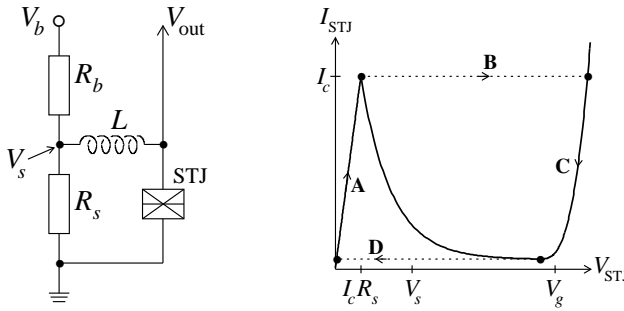


FIG. 1: Left: Circuit diagram of the relaxation oscillator. Right: Schematic *IV* characteristics of a Josephson junction with an (exaggerated) region of negative differential resistance. The four partial processes of an oscillation cycle, labeled A, B, C and D, are described in the text.

tance in the current-voltage (*IV*) characteristics. Voltage biasing the junction in that region, where R_s acts as voltage source with $R_s \ll R_n$, its operation is potentially unstable and the circuit can undergo relaxation oscillations.^{14,15,16} A relaxation oscillation cycle, which is displayed in the *IV* diagram of Fig. 1, can be separated into four phases:

- (A) Initially, when $V_s = R_s I_b > R_s I_c$ is turned on, the Josephson junction is essentially a short (supercurrent branch) and the current through L increases with a time constant $\tau_{sc} = L/R_s$ towards a value $I_{\max} = V_s/R_s$ like $I_{sc}(t) = I_{\max}(1 - e^{-t/\tau_{sc}})$ until reaching I_c within a time

$$\tau_A = -\tau_{sc} \ln \left(1 - \frac{R_s I_c}{V_s} \right). \quad (1)$$

- (B) Because the junction was current biased during phase (A) via a high-impedance L it switches now to the quasiparticle branch by developing a voltage across C_j until it is charged to V_g . The inductance holds the current constant if C_j is small enough, which means that in order to observe the “full swing” of the voltage oscillations, the inductive energy $I_c^2 L/2$ and the energy from the bias voltage $V_s^2 C_j/2$ must be sufficient to provide the charge on C_j with V_g , i.e. $I_c^2 L + V_s^2 C_j \gg (V_g - V_s)^2 C_j$ must be fulfilled. For the case of interest where $V_s \ll V_g$ this requirement is particularly true if

$$C_j \ll \frac{I_c^2 L}{V_g^2}. \quad (2)$$

Another requirement is undercritical damping of the $R_s L C_j$ circuit with $L/(C_j R_s^2) \gg 1$. However, because $R_s \ll V_g/I_c$, comparison with Eq. (2) shows that the undercritical damping condition is already implied by (2). The voltage switching time τ_B is on the order of $C_j V_g/I_c$ which is negligibly short for C_j satisfying (2).

- (C) Similarly to phase (A) the current on the quasiparticle branch decays with $\tau_{qp} = L/R_{qp}$ (where R_{qp} is the corresponding resistance in that region of the *IV* characteristics *including* the shunt R_s in series) from I_c to $I_{\min} = (V_s - V_g)/R_{qp}$ like $I_{qp}(t) = (I_c - I_{\min})e^{-t/\tau_{qp}} + I_{\min}$ until reaching zero (or a local minimum close to zero) within time

$$\tau_C = \tau_{qp} \ln \left(1 + \frac{R_{qp} I_c}{V_g - V_s} \right). \quad (3)$$

- (D) The capacitor is discharged again to zero voltage according to the conditions in phase (B), but with a subtle difference regarding final locking to the zero-voltage state, as discussed in the noise section III D.

Neglecting the short voltage switching times of phases (B) and (D), the relaxation oscillation period is given by $(\tau_A + \tau_C)$. However, when biasing a Josephson junction at $V_s \ll V_g$, the oscillation dynamics are dominated by the process in phase (A) with $\tau_A \gg \tau_C \approx O(\tau_A \frac{V_s}{V_g})$. Therefore, the relaxation oscillation frequency is essentially given by

$$f_r \approx \tau_A^{-1} = -\frac{R_s}{L} \ln^{-1} \left(1 - \frac{1}{\alpha} \right). \quad (4)$$

where $\alpha = I_b/I_c$ is the reduced bias current. A series expansion for $R_s I_c \ll V_s \ll V_g$ yields

$$f_r = \frac{R_s}{L} \left\{ \alpha - \frac{1}{2} - O\left(\frac{1}{\alpha}\right) \right\} \quad (5)$$

$$\approx \frac{V_s}{I_c L}. \quad (\alpha \gg 1) \quad (6)$$

These equations describe an almost linear analog-to-frequency converter. The same result follows from an expansion around $R_s \rightarrow 0$, relevant for the readout of a variable resistance device in place of R_s . The current-to-frequency conversion factor is

$$\frac{df_r}{dI_b} = \frac{R_s}{I_c L} + O\left(\frac{1}{I_b^2}\right). \quad (7)$$

Figure 2 shows experimental relaxation oscillation data. The amplitude of V_{out} corresponds to the gap voltage V_g , and the dynamics follow the model predictions. In the operation range $R_s I_c < V_s \leq 0.1 \cdot V_g$ the effective oscillation frequency $(\tau_A + \tau_B)^{-1}$ deviates from linearity by less than 10% (a larger operation range can also be chosen with an easy subsequent linearization of the results according to circuit calibration). Linear extrapolation of τ_A^{-1} towards $V_s = 0$ yields a frequency offset in agreement with Eq. (5).

Relaxation oscillations in Josephson junctions can be analyzed in terms of subharmonics of the Josephson frequency. This implies that the number n_ϕ of Josephson oscillations per relaxation oscillation cycle be much larger

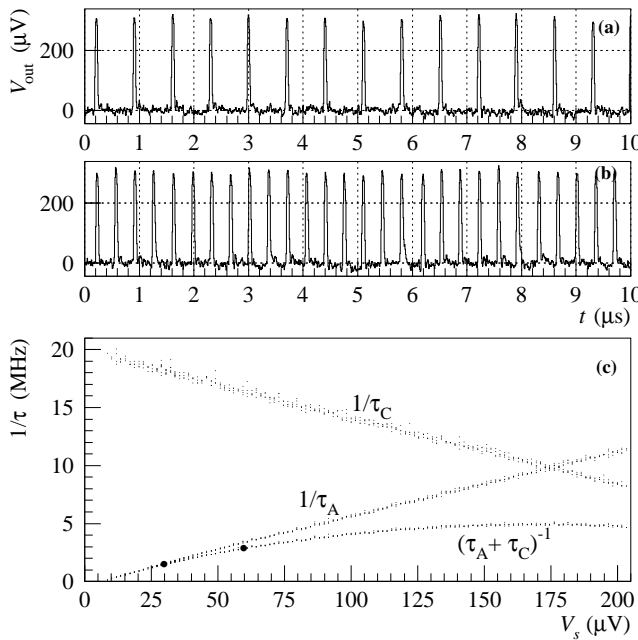


FIG. 2: Relaxation oscillation time-traces, plots (a) and (b), measured at bias voltages differing by a factor of two. Plot (c) shows the inverse of measured time constants τ_A , τ_C and of their sum as a function of V_s . The two dots in (c) correspond to the signal traces (a) and (b). Data were taken at 80 mK with an Aluminum based Josephson junction with nominally $I_c = 58.3 \mu\text{A}$ and a circuit consisting of $L = 280 \text{ nH}$, $R_s = 91 \text{ m}\Omega$.

than unity in order to prevent significant harmonic phase locking of the two oscillating processes. That sets a constraint on the frequency response and we can write

$$f_r = \frac{V_s}{\phi_0 n_\phi}, \quad (n_\phi \gg 1) \quad (8)$$

and

$$I_c L = \phi_0 n_\phi, \quad (\alpha, n_\phi \gg 1), \quad (9)$$

where ϕ_0 is the magnetic flux quantum. This argument is in line with the requirement

$$\beta_L = \frac{2\pi}{\phi_0} I_c L \gg 1 \quad (10)$$

as stated in the literature.¹⁷

Modulation of I_c by application of a magnetic field parallel to the Josephson junction results in a variation of the relaxation oscillation frequency according to Eq. (6). This offers a convenient way to tune the circuit's dynamic properties as well as to extend the operation range to lower I_b . Figure 3 shows measurements of f_r as a function of V_s for different I_c . In order to take an I_c modulation into account we denote $\kappa = I_c^0/I_c$ as the factor by which the nominal value I_c^0 may be suppressed. In the limit $T \rightarrow 0$ and equal superconductors with gap Δ the zero-field critical current¹⁸ is $I_c^0 = \pi\Delta/(2eR_n)$. Corrections

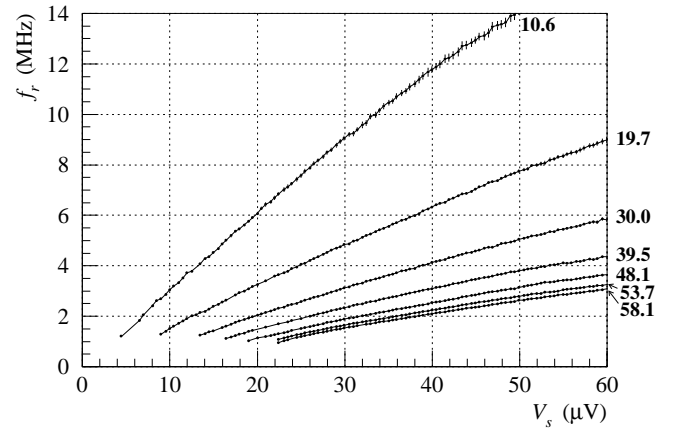


FIG. 3: Measured relaxation oscillation frequencies versus bias voltage for different I_c due to application of magnetic field. The values to the right-hand side of the curves are the effective critical currents in μA as obtained from fitting the theory to the experimental data. Device and circuit parameters are the same as in Fig. 2.

due to small gap differences are safely neglected for our analysis and we can write

$$I_c R_n \approx \frac{\pi V_g}{4\kappa}. \quad (11)$$

The dimensionless capacitance parameter β_c , which is a measure for the damping strength of the junction, is given by

$$\beta_c = (\omega_p R_n C_j)^2, \quad (12)$$

where $\omega_p = (2eI_c/\hbar C_j)^{1/2}$ is the Josephson plasma frequency. For a weakly damped and hysteretic Josephson junction we should choose β_c larger than unity. The inequality (2) in terms of Eqs. (11,12) can be rewritten as

$$\beta_c \frac{\phi_0}{2\pi} \left(\frac{4\kappa}{\pi} \right)^2 \ll I_c L, \quad (13)$$

and substituting $I_c L$ from (9) yields

$$n_\phi \gg \beta_c \frac{8\kappa^2}{\pi^3}. \quad (14)$$

This result is consistent with the condition $n_\phi \gg 1$ as we required for Eqs. (8,9).

Finally, a comparison between (10) and (13) shows that the latter is the more stringent of both conditions by the factor $\beta_c(4\kappa/\pi)^2 > 1$. Consequently, the very minimum of $I_c L$ is determined by relation (13), which constitutes, together with (14) and $\beta_c > 1$, the relevant conditions for proper observation of relaxation oscillations and which should help to choose appropriate circuit components.

III. NOISE AND RESOLUTION

A. General

In this section we list the significant current noise sources referred to the circuit input (i.e. at R_b). Special attention is paid to experimental mean fluctuations of the relaxation oscillation periods, which are denoted by $\delta\tau_r$. Assuming an analog signal which requires a bandwidth f_{bw} in order to resolve its dynamics in time (i.e. a sampling time period f_{bw}^{-1}), we measure $N = f_r/f_{bw}$ oscillations per sampled signal. The relative accuracy of a measurement improves with N as

$$\sigma_r = \frac{\delta\tau_r}{\tau_r} \frac{1}{\sqrt{N}} = \frac{\delta\tau_r}{\tau_r} \sqrt{\frac{f_{bw}}{f_r}}. \quad (15)$$

Because bias current fluctuations δI_b are linear to frequency fluctuations δf_r according to Eq. (7), we can also conclude in first order that $\delta\tau_r/\tau_r = \delta I_b/I_b$. This yields an expression for the *rms* current noise of the signal sampled at f_{bw} :

$$\langle \delta I_b \rangle_{f_{bw}} = \langle \delta I_b \rangle_{f_r} \sqrt{\frac{f_{bw}}{f_r}} = I_b \sigma_r. \quad (16)$$

Consequently, in the case of random and uncorrelated $\delta\tau_r$ fluctuations we observe a white current noise spectrum with a density

$$j_b = \frac{\langle \delta I_b \rangle_{f_{bw}}}{\sqrt{f_{bw}}} = \frac{I_b}{\sqrt{f_r}} \frac{\delta\tau_r}{\tau_r}, \quad (17)$$

apparently independent of f_{bw} . Because phase (A) of a relaxation cycle dominates the timing, we expect fluctuations in the critical current $\delta I_c \propto \delta\tau_r$ to be a major origin of $\delta\tau_r$ noise.

B. Flicker $1/f$ noise in the critical current

The critical current of Josephson junctions can fluctuate due to stochastic charge trapping at defect sites in (or close to) the barrier, which are known as “two-level fluctuators”. A sufficiently large ensemble of such fluctuators generates a $1/f$ spectrum, with significant contribution only at low frequencies. According to empirical models^{19,20} the critical current noise density j_{tlf} due to $1/f$ flicker noise can be described by

$$j_{\text{tlf}}^2 = \lambda \frac{I_c^2 T^2}{A f}, \quad (18)$$

where A is the junction area and $\lambda \approx 8.16 \times 10^{-24} \text{ m}^2/\text{K}^2$ is an average value obtained from collecting data over a wide range of different junction parameters.¹⁹ Scaling with T^2 was confirmed²⁰ for temperatures down to 90 mK (although the authors²⁰ found a higher noise level in their devices with $\lambda \approx 39 \times 10^{-24} \text{ m}^2/\text{K}^2$).

C. Critical current statistics from thermal activation

Escape from the zero-voltage state of a Josephson junction due to thermal activation is a well-known and widely studied phenomenon. It can be treated for a large variety of junction types and external conditions. For our noise analysis we can restrict ourselves to the simple “transition-state” model^{21,22} where a particle inside a well is thermally excited above the relative barrier potential and irreversibly leaves the bound state. This model is appropriate for underdamped Josephson junctions and is justified by typical device parameters and experimental conditions as given in the numerical examples (sections IV and V). Particularly, we assume intermediate operation temperatures satisfying

$$\gamma = \frac{kT}{E_J} \ll 1, \quad (19)$$

where $E_J = \hbar I_c/2e$ denotes a Josephson coupling energy, sufficient to suppress the probability of retrapping from the running state,^{23,24,25} but at the same time not too low to prevent macroscopic quantum tunneling effects. According to the model there is a nonvanishing probability for transitions from the superconducting to the resistive state at current values $I_m < I_c$. The lifetime of the zero-voltage state in a Josephson junction as a function of the reduced current $i = I/I_c$ can be expressed by^{26,27}

$$\tau_\ell^{-1}(i) = \frac{\omega_a}{2\pi} e^{-U_0/kT}, \quad (20)$$

where $\omega_a = \omega_p(1-i^2)^{1/4}$ is the “attempt frequency” of the particle in the well and $U_0 = 2E_J(\sqrt{1-i^2}-i \arccos i)$ is the relative potential height of the next barrier in the Josephson junction “washboard” potential.³⁷ The probability $P(t)$ for the junction to have switched from the superconducting to the resistive state before time t is²⁷

$$P(t) = 1 - \exp \left\{ - \int_{-\infty}^t \tau_\ell^{-1} I(t') dt' \right\}. \quad (21)$$

By assuming small fluctuations compared to I_c and using approximations in the limit $\epsilon = 1-i \ll 1$, we can solve the integral by a similar approach to Ref. 28 which yields

$$P(\epsilon) = 1 - \exp \left\{ - \frac{\omega_p \gamma}{4\pi f_r (2\epsilon)^{1/4}} \exp \left(- \frac{2(2\epsilon)^{3/2}}{3\gamma} \right) \right\}. \quad (22)$$

The mean value $\langle I_m \rangle$ of the observed critical current and its standard deviation $\langle \delta I_m \rangle$ are calculated in the Appendix and are found to be

$$\frac{\langle I_m \rangle}{I_c} \approx 1 - \frac{1}{5} (\gamma \ln \eta)^{2/3} \quad (23)$$

and

$$\frac{\langle \delta I_m \rangle}{I_c} \approx \frac{\gamma^{2/3}}{(\ln \eta)^{1/3}} \quad (24)$$

where

$$\eta = 2 \left(\frac{\omega_p}{2\pi f_r} \right)^6 \left(\frac{\gamma}{2} \right)^5. \quad (25)$$

Hence, $\langle \delta I_m \rangle$ is essentially a function of $\gamma^{2/3}$, with a weak dependence on (f_r/ω_p) . The approximations used for derivation of (23,24) are appropriate for $\eta \gg 1$. Similar results were obtained in Ref. 29. The current noise density j_m at the circuit input is, according to Eq. (17):

$$j_m = \frac{I_b}{\sqrt{f_r}} \frac{\gamma^{2/3}}{(\ln \eta)^{1/3}}. \quad (26)$$

To verify our results and to compare with other models^{30,31} of different formalism or treating different ranges of damping strength, we evaluated numerically the probabilities $P(i)$, the transition current distributions $p(i) = dP(i)/di$, and analyzed them with respect to shape, expectation value m_1 and width σ_m . We found that, within the range of allowed and reasonable model parameters, only the mean values m_1 differed quantitatively for different models, as should be expected for different initial conditions and excitation forms. However, there were insignificant differences in the distribution shapes and particularly of their widths σ_m . Therefore, Eq. 24 can be considered a good estimate for critical current fluctuations due to thermally activated escape, applicable over a wide range of $\beta_c > 1$.

D. Other noise sources

Thermal current noise from ohmic resistors is dominated by the shunt R_s and corresponds to the standard Johnson noise $j_s^2 = 4kT/R_s$. The voltage noise generated by R_s and seen by the junction is, due to $f_r \propto V_s$, not amplified and therefore equivalent to j_s at the circuit input.

The real part of a good inductance L vanishes. Therefore, L can safely be considered as a “cold resistor” without thermal noise contribution. Pickup of external magnetic noise can be shielded and becomes negligible for small coils.

Because the Josephson current is a property of the ground state of the junction, it does not fluctuate. Hence, shot noise in Josephson junctions is only due to the quasiparticle current. The relaxation oscillations within our concept are dominantly determined by processes with the junction in the superconducting state. Therefore, shot noise by itself should be negligible in our case.

However, as a consequence of the random nature of the junction phases in the quasiparticle tunneling regime, the locking to the zero-voltage state³² at the end of an oscillation cycle occurs within a time spread¹³ on the order of $\delta\tau_z \approx 2\pi\sqrt{LC_j}$. This results in an input current noise density

$$j_z = \frac{I_b}{\sqrt{f_r}} \frac{\delta\tau_z}{\tau_r}. \quad (27)$$

E. Noise conclusions

Combination of all noise sources derived above (and assumed to be uncorrelated) yields a total circuit input current noise density j_b with $j_b^2 = j_{\text{tlf}}^2 + j_m^2 + j_s^2 + j_z^2$. We make substitutions with respect to a notation of j_b in terms of the primary circuit and operation parameters L, R_s, R_n, I_c, α and T :

$$j_b^2 = c_1 \frac{(I_c R_n T)^2}{f} + c_2 \frac{\alpha I_c^{2/3} T^{4/3} L}{R_s} + c_3 \frac{T}{R_s} + c_4 \frac{\alpha^3 I_c^2 R_s}{R_n}, \quad (28)$$

where the constant coefficients c_i are orthogonal to the other parameters. Dependence on junction area A and capacitance C_j in Eq. (28) is implicit by taking the products $R_n A = \rho_n$ and $R_n C_j = \rho_n \epsilon_0 \epsilon_r / d$ to be constant in standard Josephson junctions, respectively, where ρ_n is the specific (normal) barrier resistance, ϵ_r the barrier oxide dielectric constant and d the barrier thickness. Furthermore, we have neglected the $(\ln \eta)^{1/3}$ dependence in Eq. (24) assuming $\eta \gg 1$. Hence, we can minimize the total circuit noise with respect to the parameters in Eq. (28). In particular, j_b appears to decrease with decreasing T, α (although satisfying $\alpha \gg 1$) and I_c . However, a lower I_c has to be compensated by a larger L in order to satisfy Eq. (13), for the price of lower $f_r \propto L^{-1}$ and a disadvantageous, although weak increase of noise in the second term of Eq. (28). Optimum values for R_s and R_n are found from a detailed balance of the noise contributions. Assuming, for instance, a negligible contribution from the fourth term in (28), a large R_s value seems favorable. Due to $R_s \ll R_n$, however, we see a conflict with a low noise requirement for the first term. This example implies a not too large R_n/R_s ratio.

IV. NUMERICAL ESTIMATES

In order to build a relaxation oscillation circuit we are in principle free to choose any device or circuit component and derive the remaining parameters based on optimum arguments as discussed in the previous sections. As an example we start with a Josephson junction of given area A , junction (superconducting) material and an operation temperature T . The area determines $R_n = \rho_n/A$ with a typical $\rho_n \approx 1 \text{ k}\Omega \mu\text{m}^2$ in our standard devices and $C_j = \epsilon_0 \epsilon_r A/d$ with $\epsilon_r \approx 8$ for AlO_x and $d \approx 2 \text{ nm}$. The choice of junction material is a choice of energy gaps Δ_1, Δ_2 , determining V_g, I_c^0 and E_J . It is worth noting that, according to Eq. (28), a lower $V_g \propto \kappa I_c R_n$ tends to result in a lower noise level. A lower V_g is also preferable to exclude perturbations like Fiske modes from the gap region. However, since V_g delivers the oscillation amplitude, a minimum level is required for proper resolution of the oscillating signal V_{out} . This conflict can eventually be alleviated instead by a suppression of I_c^0 by the factor κ due to application of a magnetic field, increasing the oscillation frequency which may be a desired effect. Fi-

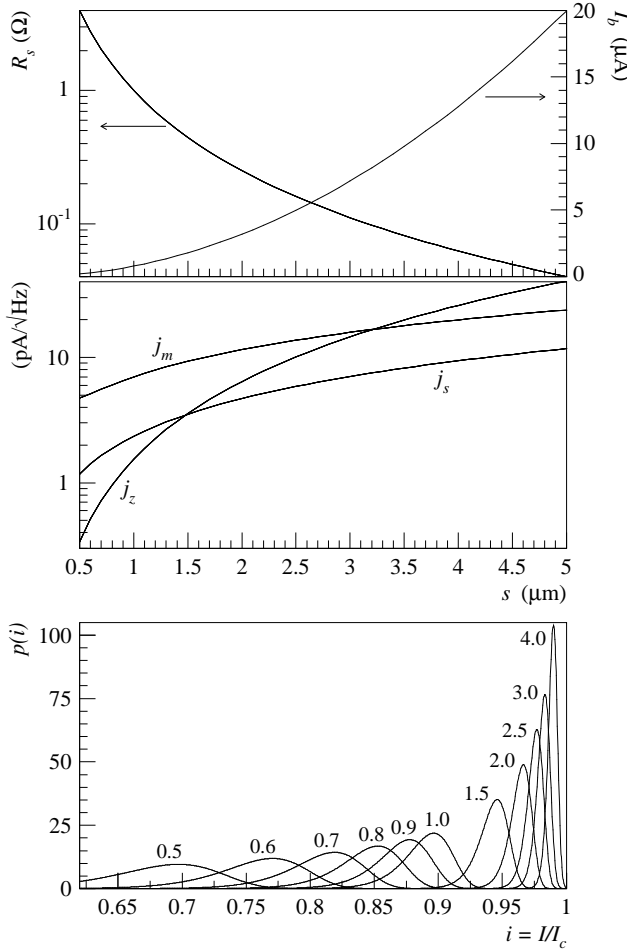


FIG. 4: Numerical calculations of R_s , I_b and the different contributions to circuit input current noise as a function of junction side length s , determined for a configuration as discussed in the text. The corresponding transition current distributions $p(i) = dP(i)/di$ due to thermally activated zero-voltage escape are shown in the bottom graph for different sizes s (identified by the numbers in units of μm adjacent to the curves.)

nally, with the choice of operation point α , the required ratio $R_s/R_n \ll 1$ and a minimum L satisfying (13), the full properties of the circuit are determined.

Figure 4 shows a numerical example of a relaxation oscillation circuit as a function of junction size (side length s), assuming an Aluminum junction ($\Delta_{\text{Al}} = 170 \mu\text{V}$), an operation temperature $T = 100 \text{ mK}$, the ratios $R_n/R_s = 10^3$, $I_c^0/I_c = 1$ and $I_b/I_c = 3$, and an effective L which is chosen 10 times larger than the minimum L_{\min} in (13). The results in Fig. 4 give an idea of the order of the parameter ranges, including the contributions from different noise sources. The flicker $1/f$ noise density (at f_r) was always at least 10^4 times lower than any other noise contribution and is therefore not shown in this example. The invariant parameters of this configuration are: $f_r = 5.23 \text{ MHz}$, $\omega_p = 151 \text{ GHz}$, $V_s = 0.80 \mu\text{V}$, $\beta_c = 28.7$, $\beta_s = \beta_c(R_s/R_n)^2 = 28.6 \times 10^{-6}$, $\beta_L = 464.5$,

$$\tau_B = 45.1 \text{ ps} \text{ and } R_n C_j = 35.4 \text{ ps.}$$

It is apparent in Fig. 4 that fluctuations due to thermally activated zero-voltage escape (i.e. current noise j_m) are the dominant noise process in the range of small devices. For illustration the corresponding distribution functions $p(i) = dP(i)/di$ of transition currents are included in Fig. 4. In spite of increasing distribution width with decreasing junction size s , the noise density decreases due to a faster decay of I_b .

As a second numerical example we calculate a realistic minimum-noise circuit configuration without leaving the range of classical dynamics of Josephson junctions as assumed for our model. We choose an Al/AlO_x/Al junction where we expect the best quality tunnel barriers and a sufficient oscillation output amplitude $V_{\text{out}} \approx 340 \mu\text{V}$. The minimum junction size is restricted by the range of validity of our model, requiring $E_J > E_C = e^2/2C_j$ and $E_J > kT$ to prevent single-electron charging or macroscopic quantum tunneling effects, respectively.³⁸ This is just satisfied with a junction of area $A = 0.1 \mu\text{m}^2 \approx (316 \text{ nm})^2$, which can be fabricated by standard e-beam lithography. An operation temperature of $T = 100 \text{ mK}$ is easily reached and maintained in modern cryostats even in the case of some moderately low dissipation in the circuit, namely $P_{\text{diss}} = I_b^2/R_s$. The values for the circuit components follow from our definitions of $\alpha = 3$, $R_n/R_s = 100$, $\kappa = 1$, $L/L_{\min} = 5$, and are listed in Table I. The results show a total input current noise as low as about $1 \text{ pA}/\sqrt{\text{Hz}}$, with the dominant contribution from thermally activated zero-voltage escape. Flicker $1/f$ noise density at f_r is at a negligible level and remains insignificant down to very low readout bandwidths f_{bw} . The total noise figure of this configuration is well competitive with the best commercial SQUID amplifiers. In addition, due to the advantage of improving noise behavior with increasing oscillation frequency, it delivers a bandwidth superior to most SQUID systems.

It is clear that the operation point for the current or voltage biased device under test is fixed to I_b or V_s in this example. For devices requiring different bias values (as in Ref. 33) the circuit components have to be adapted with respect to the specifications.

V. POSSIBLE APPLICATIONS

We have developed the relaxation oscillation analog-to-frequency converter primarily for readout of cryogenic radiation detectors.³⁴ The aim was to overcome problems or limitations in scaling to large number pixel readout. Besides the outstanding noise properties, a particularly nice feature of the relaxation oscillation circuit is its potential for simple implementation into a frequency-domain multiplexing scheme by tuning the oscillation frequencies of the individual analog-to-frequency converters to well separated values, and then using one single line to read them out. It should be taken into account, however, that a signal excursion from a detector generates a frequency shift,

TABLE I: List of component and operation parameter values of a relaxation oscillation circuit optimized with respect to minimum input current noise. Initial conditions are described in the main text.

A (μm^2)	R_n (Ω)	R_s (Ω)	C_j (fF)	I_c (nA)	I_b (nA)	V_s (μV)	L (μH)	β_c	β_L	f_r (MHz)	ω_p (GHz)	τ_B (ps)	$\delta\tau_z$ (ns)	I_m/I_c	$\delta I_m/I_c$	j_{tf} (fA/ $\sqrt{\text{Hz}}$) ^a	j_m (fA/ $\sqrt{\text{Hz}}$) ^a	j_s (fA/ $\sqrt{\text{Hz}}$) ^a	j_z (fA/ $\sqrt{\text{Hz}}$) ^a
0.1	10^4	10^2	3.54	25.0	75.1	7.51	2.87	26.9	218	104.5	146.6	44.9	0.63	0.56	0.098	0.002 ^b	965	235	363

^aThese units refer to all four current noise density terms.

^bValue taken at f_r .

which should not overlap with a neighboring oscillator in the simplest case. A more sophisticated scheme could lock into the “dark” (no detector signal) characteristic frequencies and, upon disappearance of one channel due to an analog detector signal, remove the other frequency bands in order to recover the signal of interest.³⁹

To test and demonstrate the working principle we have measured the response of a SINIS microcalorimeter³⁵ to irradiation with 6 keV X-rays, using a relaxation oscillation circuit readout. The detector which replaced R_b was voltage biased. Figure 5 shows the results of an X-ray event. The circuit and device parameters were: $L = 48\text{nH}$, $R_s = 91\text{m}\Omega$, junction size $s = 15\text{\mu m}$ and effective critical current $I_c = 7.28\text{\mu A}$ ($\kappa = 8$). The detector’s “dark” (or bias) current was $I_b^0 = 17.5\text{\mu A} = 2.4I_c$, the measured analog signal peak current was $I_b^1 = 46.4\text{\mu A}$, as shown in Fig. 5d. The relaxation oscillation frequencies from Fig. 5c, taken at the same operation point and conditions, were $f_r^0 = 4.47\text{MHz}$ and $f_r^1 = 12.1\text{MHz}$, respectively. Taking into account the conversion factor $\text{d}f_r/\text{d}I_b = 260\text{kHz}/\text{\mu A}$, see Eq. (7), the analog and the frequency-modulated signal are perfectly compatible quantitatively as well as qualitatively (pulse shape). The noise level is about the same in both cases and is due to detector noise. The circuit noise alone is estimated to contribute about 0.3\mu A rms integrated over full bandwidth up to f_r . We should say that the microcalorimeter device and circuit configuration are by no means optimal in this example, they are rather a preliminary choice of available components. Primarily, these results are of illustrative nature, demonstrating the principle and feasibility of cryogenic detector readout.

Other possible applications for relaxation oscillation based analog-to-frequency conversion can be, in a wider sense, considered for any type of cryogenic device operated at relatively low bias levels, exhibiting small variations of its electronic properties or actively delivering small analog signals. A list may include quantum dots and wires, single-electron devices and quantum Hall structures, to name a few. Due to the large bandwidth, the readout method is also attractive for detection of fast processes like quantum noise or background charge fluctuations. The resistors R_b and R_s in our scheme just represent a current and a voltage source, respectively, and can be replaced by the device of choice.

It is important to note, however, that the oscillator junction characteristics (essentially represented by I_c)

may slightly vary from cooldown to cooldown and therefore cause a measurable spread in the conversion factor (7). Therefore, the circuit is unfortunately not appro-

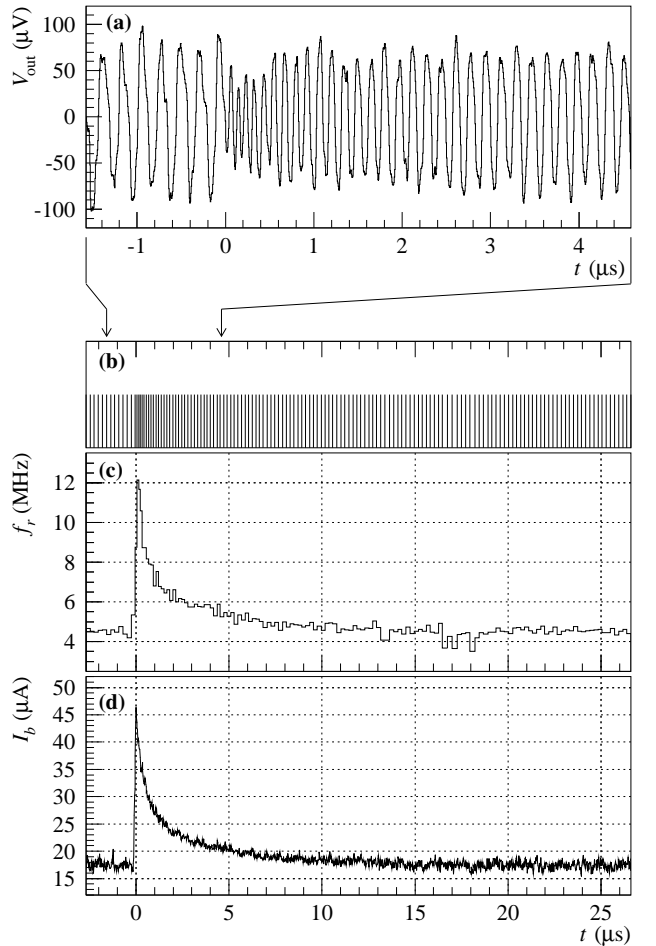


FIG. 5: (a) Response of the relaxation oscillation circuit modulated due to a 6 keV X-ray event in a SINIS detector at 80mK . The sinusoidal shape and reduced amplitude of the oscillations are due to band-pass filtering at the post-amplification stage. (b) Rectified oscillator signal where each line represents the position of an oscillation cycle maximum (note the larger time scale, applying to all three lower plots). (c) Inverse oscillation periods as a function of time, equivalent to a time-dependent frequency f_r . (d) Analog signal from the same detector measured with conventional electronics and taken at corresponding experimental conditions.

priate for absolute measurements on a level as required e.g. by metrologists.

As a concluding experiment we propose a setup for high-precision thermometry at low temperatures, replacing the classical four-point measurement on thermistors. The temperature-sensitive element would typically replace R_s to minimize dissipation. The difficulty of applying small analog excitations and detecting low output levels (across long wires), competing with noise, is circumvented by directly “digitizing” the small signal very close to the sensor with a low-noise converter. It is clear that this thermometer readout can only be operated in a limited temperature range (presumably one order of magnitude) where the junction dynamics (fluctuations, switching probabilities) are sufficiently insensitive to T variations.

VI. CONCLUSIONS

We have investigated the feasibility of a cryogenic low-noise analog-to-frequency converter with acceptable linearity over a broad range of circuit and operation parameters. The dynamical behavior can be well described by simple circuit theory and classical models of the single Josephson junction involved. Their agreement with experimental data is perfect. We have presented a thorough analysis of noise sources, where fluctuation processes in the Josephson junction appear to usually dominate the circuit’s noise figure for typical configurations and experimental conditions. The inherent broadband operation paired with very good noise performance offers a versatile system for a wide range of applications. As one possible example we have demonstrated the readout of a cryogenic microcalorimeter exposed to X-rays. Implementation into a multiplexing scheme was discussed and needs to be experimentally tested for a large channel-number readout.

Acknowledgments

We are grateful to Eugenie Kirk for excellent device fabrication, to Philippe Lerch and Alex Zehnder for valuable and stimulating discussions, and to Fritz Burri for technical support.

*

APPENDIX A

For the analysis of noise due to thermally activated zero-voltage escape an evaluation of the central moments

of the probability density function $p(i) = dP(i)/di$ is required, yielding expectation value $m_1 = \int i p(i) di$ and variance $m_2 = \int (i - m_1)^2 p(i) di$, where $P(i)$ is given by Eq. (22) and $\sigma_m = \sqrt{m_2}$ subsequently denotes the standard deviation. Analytical integration can be circumvented, however, by approximating $p(i)$ with a Gaussian distribution and solving for the appropriate values satisfying $P(m_1) = 0.5$ and $P(m_1 \pm \sigma_m) = 0.5\{1 \pm \text{erf}(1/\sqrt{2})\}$, respectively. A general solution of $P(m) = h$ is

$$m = \frac{1}{8} \left\{ 2\gamma W \left(\frac{\eta}{\ln(1-h)^6} \right) \right\}^{2/3}, \quad (\text{A1})$$

where $\eta = 2(\omega_p/2\pi f_r)^6(\gamma/2)^5$ and W is the Lambert function satisfying $W(x) \cdot \exp(W(x)) = x$. An asymptotic expansion of W for $(x \rightarrow \infty)$ can be written as $W(x) = \ln x - \ln(\ln x)$, where higher order terms are suppressed. Setting $h = 0.5$ in Eq. (A1) yields the expectation value

$$\frac{\langle I_m \rangle}{I_c} = m_1 \approx 1 - \frac{1}{8} \left(2\gamma \ln \frac{9\eta}{\ln(9\eta)} \right)^{2/3}.$$

In the limit ($\eta \rightarrow \infty$) this expression approaches

$$\frac{\langle I_m \rangle}{I_c} \approx 1 - \frac{1}{8} (2\gamma \ln \eta)^{2/3}. \quad (\text{A2})$$

Correspondingly, for $\langle \delta I_m \rangle / I_c = \sigma_m$ we find an expansion

$$\frac{\sigma_m}{\frac{1}{8} (2\gamma)^{2/3}} \approx \frac{4.73}{(\ln \eta)^{1/3}} + \frac{1.58 \ln(\ln \eta) - 10.15}{(\ln \eta)^{4/3}},$$

which, for ($\eta \rightarrow \infty$), approaches

$$\begin{aligned} \frac{\langle \delta I_m \rangle}{I_c} &\approx \frac{1}{8} (2\gamma)^{2/3} \frac{4.73}{(\ln \eta)^{1/3}} \\ &\approx 0.94 \frac{\gamma^{2/3}}{(\ln \eta)^{1/3}}. \end{aligned} \quad (\text{A3})$$

If m_1 significantly deviates from unity the approximation

$$\frac{\langle \delta I_m \rangle}{\langle I_m \rangle} \approx \frac{\gamma^{2/3}}{(\ln \eta)^{1/3}} + \frac{3}{16} \gamma^{4/3} (\ln \eta)^{1/3} + \mathcal{O}(\gamma^2 \ln \eta) \quad (\text{A4})$$

describes the relative distribution width of transition current fluctuations.

¹ R. J. Schoelkopf, P. Wahlgren, A. A. Kozhevnikov, P. Delsing, and D. E. Prober, *Science* **280**, 1238 (1998).

² K. Segall, K. W. Lehnert, T. R. Stevenson, R. J.

Schoelkopf, P. Wahlgren, A. Aassime, and P. Delsing, *Appl. Phys. Lett.* **81**, 4859 (2002).

³ W. Lu, Z. Ji, L. Pfeiffer, K. W. West, and A. J. Rimberg, *Nature (London)* **423**, 422 (2003).

⁴ J. Bylander, T. Duty, and P. Delsing, *Nature (London)* **434**, 361 (2005).

⁵ P. K. Day, H. G. LeDuc, B. A. Mazin, A. Vayonakis, and J. Zmuidzinas, *Nature (London)* **425**, 817 (2003).

⁶ D. R. Schmidt, K. W. Lehnert, A. M. Clark, W. D. Duncan, K. D. Irwin, N. Miller, and J. N. Ullom, *Appl. Phys. Lett.* **86**, 053505 (2005).

⁷ T. R. Stevenson, F. A. Pellerano, C. M. Stahle, K. Aidala, and R. J. Schoelkopf, *Appl. Phys. Lett.* **80**, 3012 (2002).

⁸ K. D. Irwin and K. W. Lehnert, *Appl. Phys. Lett.* **85**, 2107 (2004).

⁹ D. W. Gerdt, M. V. Moody, and J. L. Paterson, *J. Appl. Phys.* **50**, 3542 (1979).

¹⁰ I. P. Nevirkovets, *Supercond. Sci. Technol.* **11**, 711 (1998).

¹¹ M. Mück, H. Rogalla, and C. Heiden, *Appl. Phys. A* **47**, 285 (1988).

¹² S. A. Gudoshnikov, Yu. V. Maslennikov, V. K. Semenov, O. V. Snigirev, and A. V. Vasiliev, *IEEE Trans. Magn.* **25**, 1178 (1989).

¹³ D. J. Adelerhof, H. Hijstad, J. Flokstra, and H. Rogalla, *J. Appl. Phys.* **76**, 3875 (1994).

¹⁴ I. K. Albegova, B. I. Borodai, I. K. Yanson, and I. M. Dmitrenko, *Zh. Tekh. Fiz.* **39**, 911 (1969), [Sov. Phys. Tech. Phys. **14**, 681 (1969)].

¹⁵ F. L. Vernon and R. J. Pedersen, *J. Appl. Phys.* **39**, 2661 (1968).

¹⁶ N. Calander, T. Claeson, and S. Rudner, *Phys. Scr.* **25**, 837 (1982).

¹⁷ C. B. Whan, C. J. Lobb, and M. G. Forrester, *Appl. Phys. Lett.* **77**, 382 (1995).

¹⁸ V. Ambegaokar and A. Baratoff, *Phys. Rev. Lett.* **10**, 486 (1963).

¹⁹ D. J. Van Harlingen, T. L. Robertson, B. L. T. Plourde, P. A. Reichardt, T. A. Crane, and J. Clarke, *Phys. Rev. B* **70**, 064517 (2004).

²⁰ F. C. Wellstood, C. Urbina, and J. Clarke, *Appl. Phys. Lett.* **85**, 5296 (2004).

²¹ H. A. Kramers, *Physica* **7**, 284 (1940).

²² P. Hänggi, P. Talkner, and M. Borkovec, *Rev. Mod. Phys.* **62**, 251 (1990).

²³ J. M. Kivioja, T. E. Nieminen, J. Claudon, O. Buisson, F. W. J. Hekking, and J. P. Pekola, *Phys. Rev. Lett.* **94**, 247002 (2005).

²⁴ J. Männik, S. Li, W. Qiu, W. Chen, V. Patel, S. Han, and J. E. Lukens, *Phys. Rev. B* **71**, 220509 (2005).

²⁵ V. M. Krasnov, T. Bauch, S. Intiso, E. Hürfeld, T. Akazaki, H. Takayanagi, and P. Delsing, *Phys. Rev. Lett.* **95**, 157002 (2005).

²⁶ P. A. Lee, *J. Appl. Phys.* **42**, 325 (1971).

²⁷ T. A. Fulton and L. N. Dunkleberger, *Phys. Rev. B* **9**, 4760 (1974).

²⁸ J. Kurkijärvi, *Phys. Rev. B* **6**, 832 (1972).

²⁹ O. V. Snigirev, *IEEE Trans. Magn.* **19**, 584 (1983).

³⁰ B. Carmeli and A. Nitzan, *Phys. Rev. Lett.* **51**, 233 (1983).

³¹ A. Barone, R. Cristiano, and P. Silvestrini, *J. Appl. Phys.* **58**, 3822 (1985).

³² T. A. Fulton, *Appl. Phys. Lett.* **19**, 311 (1971).

³³ M. Furlan, E. Kirk, and A. Zehnder, *physics/0507005*, *Nucl. Instrum. Meth. A* (2006), to be published.

³⁴ N. E. Booth, B. Cabrera, and E. Fiorini, *Annu. Rev. Nucl. Part. Sci.* **46**, 471 (1996).

³⁵ M. Furlan, E. Kirk, and A. Zehnder, *physics/0507003*, *Nucl. Instrum. Meth. A* (2006), to be published.

³⁶ R. L. Kautz and J. M. Martinis, *Phys. Rev. B* **42**, 9903 (1990).

³⁷ The argument in the exponent of Eq. (20) is in general notation $(-U_0/E_0)$ with $E_0 \approx \max\{kT, \hbar\omega_a/2\pi\}$ in first approximation, taking into account the crossover between classical and quantum limits. In the range of interest ($\omega_a \rightarrow 0$ for $i \rightarrow 1$) the excitation E_0 is dominated by kT .

³⁸ The phase diffusion model in Ref. 36 does not significantly alter the switching behavior (and thereby the noise) of our dynamical circuit even for moderate E_J/E_C ratios, as long as β_c is sufficiently large.

³⁹ In case of frequency band overlap, the signal, which is only partially recovered, can be reconstructed from a decent knowledge of the expected pulse shape.